the pulse, an increase in the efficiency of mass utilization may be expected. Thus, future experiments should be done with higher power, shorter pulse lasers. The advantage of a short-pulse system is that the thrusting time will be much greater than the pulse time, and quasi-steady thrust may be obtainable by a series of short laser pulses such that each succeeding thrusting pulse begins before the previous one ends. It is necessary, however, to design an efficient propellant feed system to complete this system.

References

[1] Kantrowitz, A. R., "The Relevance of Space," *Aeronautics & Astronautics*, Vol. 9, No. 3, March 1971, p. 35.

[2] Kantrowitz, A. R., "Propulsion to Orbit by Ground-Based Lasers," *Aeronautics & Astronautics*, Vol. 10. No. 5, May 1972, p. 74.

[3] Rom, F. E. and Putre, H. A., "Laser Propulsion," TM-X-2510, April 1972, NASA.

[4] Pirri, A. N. and Weiss, R. F., "Laser Propulsion," AIAA Paper 72-719, Boston, Mass., 1972.

[5] Basov, N. G., Gribkov, V. A., Krokhin, O. N., and Sklizkov, G. V., "High Temperature Effects of Intense Laser Emission Focused on a Solid Target," *Soviet Physics—JETP*, Vol. 27, No. 4, Oct. 1968, p. 575.

[6] Pirri, A. N., Schlier, R., and Northam, D., "Momentum Transfer and Plasma Formation Above a Surface with a High-Power CO_2 Laser," *Applied Physics Letters*, Vol. 21, No. 3, Aug. 1972, pp. 79–81.

[7] Gregg, D. W. and Thomas, S. J., "Momentum Transfer Produced by Focused Laser Giant Pulses," *Journal of Applied Physics*, Vol. 37, No. 7, June 1966, pp. 2787–2789.

[8] Gregg, D. W. and Thomas, S. J., "Kinetic Energies of Ions Produced by Laser Giant Pulses," *Journal of Applied Physics*, Vol. 37, No. 12, Nov. 1966, pp. 4313–4316.

[9] Zel'dovich, Y. B. and Raizer, Y. P., *Physics of Shock Waves and High-Temperature Hydrodynamic Phenomena*, Academic Press, New York, 1966, pp. 258–283.

[10] Lowder, J. E., Lencioni, D. E., Hilton, T. W., and Hull, R. J., "High-Energy Pulsed CO_2 Laser-Target Interaction in Air," *Journal of Applied Physics*, Vol. 44, No. 6, June 1973, p. 2759.

[11] Pirri, A. N., "Theory for Momentum Transfer to a Surface with a High-Power Laser," *The Physics of Fluids*, Vol. 16, No. 9, Sept. 1973, p. 1435.

[12] Hall, R. B., Maher, W. E., and Wei, P. S. P., "An Investigation of Laser-Supported Detonation Waves," AFWL-TR-73-28, June 1973, Air Force Weapons Lab., N.Mex.

[13] Hettche, L. R., Schriempf, J. T., and Stegman, R. L., "Impulse Reaction Resulting from the In-Air Irradiation of Aluminum by a Pulsed CO_2 Laser," *Journal of Applied Physics*, Vol. 44, No. 9, Sept. 1973, p. 4079.

[14] Barchukov, A. I., Bunkin, F. V., Konov, V. I., and Prokhorov, A. M., "Low-Threshold Breakdown of Air near a Target by CO_2 Radiation, and the Associated Large Recoil Momentum," *JETP Letters*, Vol. 17, No. 8, April 20, 1973, p. 294.

[15] Buonadonna, V. R., Knight, C. J., and Hertzberg, A., "The Laser Heated Wind Tunnel," *AIAA Journal*, Vol. 11, No. 11, Nov. 1973, pp. 1457–1458.

SEPTEMBER 1974 AIAA JOURNAL VOL. 12, NO. 9

Heat Pipe Model Accounting for Variable Evaporator and Condenser Lengths

C. L. WILLIAMS*
Westinghouse Electric Corporation, Pittsburgh, Pa.

AND

G. T. COLWELL†
Georgia Institute of Technology, Atlanta, Ga.

A correlation model is established for the steady-state performance of a horizontal heat pipe operating below the capillary limited heat rate and with internally self adjusting evaporator and condenser lengths. The length along which condensation occurs is found to depend on the axial vapor Reynolds number. The partially saturated evaporator length, and the corresponding length along which evaporation occurs is found to depend on the detail wick geometry and the evaporator meniscus radius. These dependencies are corroborated by experimental data from a cylindrical heat pipe with working fluids of water and methanol. The experimental wick consists of two layers of 100 mesh stainless steel screen separated by a thin liquid region. Comparison of correlation predictions to experimental results of this study and others show agreement to within 15%.

Nomenclature

A_w = wick total cross-sectional area, ft^2
f = function
h_{vl} = latent heat of vaporization, btu/lbm
K_{eff} = effective wick thermal conductivity for two layers of screen (btu/hr ft °R)
K_l = liquid thermal conductivity, (btu/hr ft °R)
K_s = wick solid thermal conductivity, (btu/hr ft °R)
K_w = effective wick thermal conductivity for one layer of screen, (btu/hr ft^2 °R)
K = wick friction factor (inverse permeability), 1/ft^2
l_{eff} = liquid effective frictional length, ft
l = design length, ft
L = active length, ft
$\dot{m}$ = mass flow rate, lbm/hr
n = number of layers of screen
P = pressure, lbf/ft^2 absolute
$\dot{Q}_e$ = evaporator heat-transfer rate, btu/hr
r_c = wick pore radius, ft
r_m = evaporator meniscus radius, ft
r_v = vapor space radius from heat pipe axis, ft
r_w = outer radius of wick, ft
r_{ws} = wick-solid radius (one-half wire diameter for mesh screen), ft
Re = Reynolds number
$\bar{T}_{ew}$ = evaporator average temperature at outer wick surface, °R

Received September 10, 1973; revision received February 26, 1974. This work was performed on a Ph.D. thesis during graduate study at Georgia Institute of Technology.

Index categories: Heat Conduction; Thermal Modeling and Experimental Thermal Simulation.

* Senior Engineer, Bettis Atomic Power Laboratory.

† Associate Professor, School of Mechanical Engineering.

T_c = condenser sink temperature, °R
T_{cw} = condenser average temperature at outer wick surface, °R
T_o = heat pipe operating temperature, °R
U_c = unit conductance between outer wick surface and condenser sink, (btu/hr ft^2 °R)
δ_e = evaporator effective wick thickness, ft
μ = dynamic viscosity lbm/ft sec
ρ = density, lbm/ft^3
σ = surface tension, lbf/ft
ϕ = wetting angle, degrees

Subscripts

a = adiabatic
c = condenser
e = evaporator
l = liquid
l, c = liquid, condenser
l, e = liquid, evaporator
v = vapor
v, c = vapor, condenser
v, e = vapor, evaporator

Introduction

HEAT pipe design has been the topic of investigations by Cotter[4] Kunz, [6,7] and many others.[12,15] Typical assumptions for these analytical models include: 1) operation at the capillary limited maximum heat rate; 2) completely saturated wicks; and 3) evaporation (condensation) along the entire design length of heat addition (heat removal). Computations based on these models are useful but are not adequate at relatively low fluxes, particularly when active evaporator and condenser lengths are less than design lengths.

Chi[2] analyzed a cryogenic heat pipe operating below the capillary limited maximum heat rate. He developed expressions for determining both radial and axial temperature distributions in the evaporator and condenser sections. The expressions take into account liquid property variations.

The subject of partially saturated wicks has been studied by Roberts,[9] Chun,[3] and others. Roberts'[9] momentum analysis is typical in that it considers vertical heat pipe operation only at or nearly the capillary limited maximum heat rate and defines a partially saturated wick as one in which the liquid-vapor interface is step-wise recessed in a direction normal to the heat pipe axis with the entire evaporator length exposed to liquid.

The thermal analysis by Sun[13] predicted self adjusting evaporator and condenser lengths. The mechanism for these variations was axial conduction of heat along the heat pipe shell. Sun showed these variations are negligible for thin-wall shells of low thermal conductivity. The vapor momentum analysis by Bankston[1] indicated that flow reversal could occur in the condenser section. The partial length of reversed flow was dependent upon the vapor flow characteristics (such as Reynolds number).

In this paper, a correlation theory is developed which takes account of: 1) both momentum and thermal analysis; 2) heat pipe operation below the capillary limited maximum heat rate; 3) variation of the evaporator length due to a nonisotropic wick which is partially saturated; and 4) variation of the length along which condensation occurs due to vapor flow characteristics. The condenser length model can be applied to any heat pipe and the evaporator length model identifies the parameters controlling evaporator length change. In order to provide evidence for the length correlations, experimental data were obtained from a horizontal heat pipe with working fluids of water and methanol.

Experimental

Equipment

The heat pipe shell, Fig. 1, was fabricated from a $\frac{3}{4}$-in.-diam and 18-in. long tube of 304 stainless steel. The wick consisted of two layers of 100 mesh stainless steel screen separated by a thin liquid region (see Table 1 for a listing of geometric parameters). The condenser calorimeter was constructed from a 1-in.-diam and 5-in. long stainless steel pipe which was mounted concentric to the heat pipe shell and sealed at each end with header chambers. The evaporator section was formed by wrapping an electric resistance heating coil helically over the evaporator length while the adiabatic section was covered with fiberglass insulation. Pressure transducers were attached to the heat pipe shell at the ends of the adiabatic section and thermocouples were attached along the shell outer wall, in the vapor region, and between the screen layers. The wick thermocouples (36 gage) provided a thin liquid region between the layers of screen. The location of various sensing devices is shown in Fig. 1.

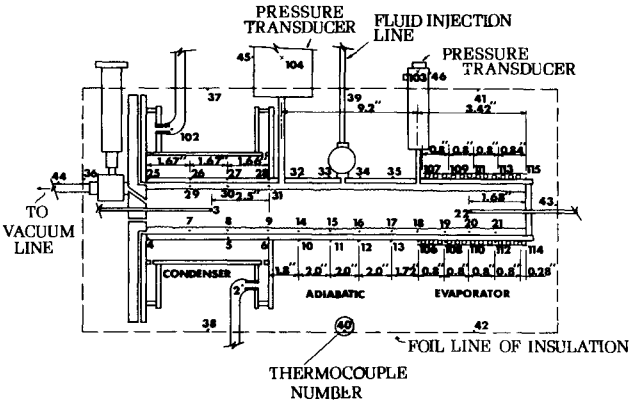

Fig. 1 Experimental heat pipe.

Procedure

Following wick cleaning and assembling, a vacuum was first drawn on the heat pipe to a pressure of 10 μ. Preheated working fluid (water or methanol) was then injected into the pipe from a burette. The amount of fluid injected was estimated to saturate the wick with liquid and fill the vapor region with vapor. No excess fluid was injected. Heat transfer was initiated by forcing prechilled cooling water through the condenser jacket and then applying a voltage across the evaporator heating element.

The heat-pipe operating point was changed by changing the power delivered to the evaporator heating coil, changing the water flow rate through the condenser cooling jacket, or changing the cooling water inlet temperature. Once the change was initiated, the system was permitted to reach steady state, then temperatures, pressures, calorimeter flow rate, and coil power were recorded. The corresponding externally independent parameters were $\dot{Q}_e$, power delivered to the evaporator, U_c, condenser unit conductance from the outer wick surface to the heat sink, and T_c, the condenser sink temperature. Further details on equipment and procedure are given in Ref. 14.

Table 1 Geometric parameters of experimental heat pipe

Name	Symbol	Value in. or no.
evaporator length	l_e	3.36
adiabatic length	l_a	9.64
condenser length	l_c	5.00
inside wick radius	r_v	0.298
outside wick radius	r_w	0.326
wick pore radius	r_c	0.00275
wick-solid radius	r_{ws}	0.00225
number of screen layers	n	2

Table 2 Operating data

Fluid	Test	Q_e btu/hr	T_c °F	U_c btu/hr ft² °R	T_o °F
Water	1	155.0	69.74	236.46	93.55
	2	230.3	70.43	234.89	102.37
	3	331.0	71.30	235.25	111.11
	4	339.6	72.13	219.67	118.14
	5	172.7	70.33	243.23	97.29
	6	249.9	71.15	232.48	103.82
	7	349.9	72.51	220.86	114.56
	8	167.5	70.98	198.70	100.57
	9	247.9	72.90	176.19	110.25
Methanol	10	52.2	67.67	135.71	93.09
	11	90.8	70.30	133.91	104.26
	12	39.0	66.70	229.62	88.54
	13	50.8	67.03	183.53	91.91
	14	68.2	68.07	156.36	97.87
	15	93.7	68.77	146.75	103.72
	16	52.7	54.66	121.28	85.97
	17	71.9	57.60	116.25	93.10
	18	80.8	60.44	140.43	100.29
	19	24.9	46.95	202.59	73.64
	20	66.1	48.81	138.85	86.07
	21	20.6	42.97	186.66	71.51

Experimental Results

Operating data are tabulated in Table 2. Included with externally independent parameters is T_o, the observed operating temperature. Typical axial temperature distributions are shown in Fig. 2. Near isothermal conditions were observed along the adiabatic shell wali. Vapor temperatures for Test 9 coincided with values along the adiabatic wall. The condenser vapor temperature of Test 20 agreed with the condenser wall value, suggesting negligible radial heat transfer near the axial position of thermocouple T_3. High evaporator wall temperatures (T_{113}) were observed for both tests. This suggests that wick drying had occurred. If drying did exist, it must have been a partial drying, since evaporator vapor temperatures were nearly equal to the corresponding adiabatic wall temperatures.

Correlation Model

For the present system a momentum equation reduces to a pressure balance over the fluid cycle of evaporation, vapor flow, condensation, and liquid flow. Using the approach of Kunz,[6,7] this balance is (see Fig. 3)

$$(P_{l,e}-P_{v,e})+(P_{v,e}-P_{v,c})+(P_{v,c}-P_{l,c})+(P_{l,c}-P_{l,e})=0 \quad (1)$$

Neglecting inertial forces (Ref. 14) and characterizing the evaporator liuqid-vapor interface by a single meniscus radius gives

$$P_{l,e}-P_{v,e}=-(2\sigma/r_m) \quad (2)$$

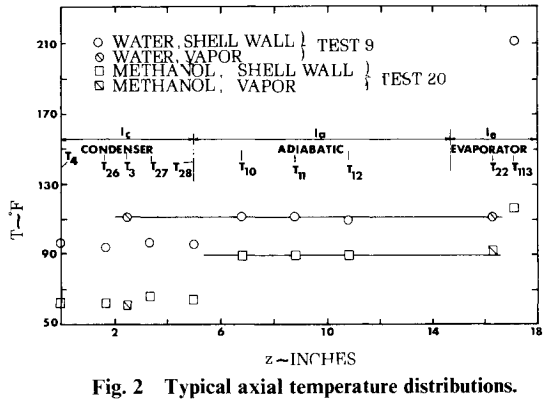

Fig. 2 Typical axial temperature distributions.

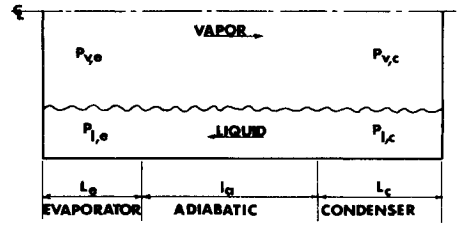

Fig. 3 Correlation model.

The vapor pressure drop is assumed to be negligible for low velocity vapor flow.[6,7,14] The pressure drop across the liquid-vapor interface in the condenser section is assumed to be negligible[4,6,7] which suggests this interface to be a flat interface. Using Darcy's law for liquid flow[6,7,10] gives

$$P_{l,c}-P_{l,e}=K(\mu_l/\rho_l)(\dot{m}/A_w)l_{\text{eff}} \quad (3)$$

where l_{eff} is the effective frictional length of the liquid flow and K is the inverse of permeability. Equation (3) is simplified by assuming mass flow to be uniform and radial at the liquid-vapor interface of both the evaporator and condenser.[4,6,7] It is further assumed that all energy goes to phase change.[2,4,6,7] These assumptions provide the simple relations

$$l_{\text{eff}}=\tfrac{1}{2}L_e+l_a+\tfrac{1}{2}L_c \quad (4)$$

and

$$\dot{m}=\dot{Q}_e/h_{v,l} \quad (5)$$

respectively.

Substitution of Eqs. (2–5) into Eq. (1) and neglecting the second and third terms of Eq. (1) yields

$$\frac{r_m}{r_c}=2\left\{\left[\frac{\rho_l\sigma h_{v,l}}{\mu_l}\right]\left[\frac{\pi(r_w^2-r_v^2)}{\dot{Q}_e}\right]\Big/Kr_c\left[\tfrac{1}{2}L_e+l_a+\tfrac{1}{2}L_c\right]\right\} \quad (6)$$

where the pore radius r_c is used to characterize the wire mesh opening size.

The internal heat balance is modeled by considering the only significant thermal resistances to be those for simple radial conduction through the wick.[14] This model yields

$$\dot{Q}=[\bar{T}_{ew}-\bar{T}_{cw}]\Big/\left[\ln\frac{r_w}{r_{ve}}\Big/2\pi K_{\text{eff}}L_e+\ln\left(\frac{r_w}{r_{vl}}\right)\Big/2\pi K_{\text{eff}}L_c\right] \quad (7)$$

where $\bar{T}_{ew}$ and $\bar{T}_{cw}$ are the average temperatures at the wick outer radius r_w along the active lengths L_e and L_c of the evaporator and condenser sections, respectively, K_{eff} is the wick effective thermal conductivity, and r_{ve} is the radius, from the heat pipe axis, of the liquid-vapor interface in the evaporator section. In order to provide interpretations of the parameters of Eqs. (6) and (7), the condenser and evaporator sections are examined individually.

Condenser Section

The fluid flow path in the condenser is modeled as that of vapor flowing axially into a long cavity with porous walls. The

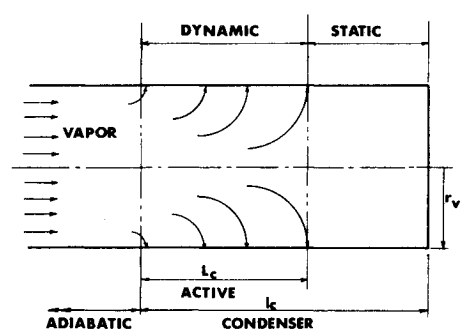

Fig. 4 Condenser active length model.

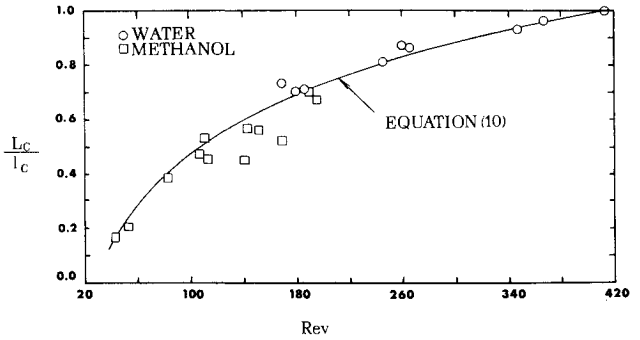

Fig. 5 Condenser active length vs axial vapor Reynolds number.

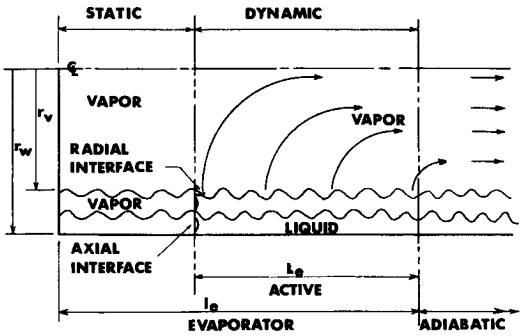

Fig. 6 Evaporator active length model.

length of the cavity is divided into two regions, one with vapor flowing and one with the vapor static (see Fig. 4). For low axial momentum entering the cavity, the flow is considered quenched; i.e., the vapor ceases to flow axially before reaching the design length of the condenser. For high axial momentum the flow is considered unquenched; i.e., the entire design length is filled with flowing vapor. This model suggests a relation of the form

$$L_c/l_c = \text{function}(Re) \tag{8}$$

where L_c/l_c is the ratio of active to design length of the condenser, and Re is the vapor axial Reynolds number at the cavity entrance given by

$$Re = (2/\pi)(\dot{Q}_e/r_v \mu_v h_{vl}) \tag{9}$$

Consideration of the data taken in this investigation, see Fig. 5, suggests the relations

$$L_c/l_c = 1.245\{0.3 \ln[(2/\pi)(\dot{Q}_e/r_v \mu_v h_{vl})] - 1.0\} \tag{10}$$

for

$$28 < (2/\pi)(\dot{Q}_e/r_v \mu_v h_{vl}) < 408 \tag{11}$$

and

$$L_c/l_c = 1.0 \tag{12}$$

for

$$(2/\pi)(\dot{Q}_e/r_v \mu_v h_{vl}) \geqq 408 \tag{13}$$

For this correlation, the active length L_c was evaluated from the measured parameters of heat-transfer rate and vapor and outer shell wall temperatures.

The heat flow is modeled as simple radial conduction. On this basis, the wall temperature $\bar{T}_{cw}$ is dependent upon T_c and U_c. Hence the condenser contribution to Eq. (7) is expressed by

$$T_o - T_c = \dot{Q}_e[\ln(r_w/r_c)/2\pi k_{\text{eff}} L_c + 1/U_c 2\pi r_w L_c] \tag{14}$$

where T_o is the vapor temperature at the liquid-vapor interface along the active length.

The wick effective thermal conductivity is evaluated by considering parallel and series conduction through a wick formed by layers of screen separated by a thin liquid region. This model gives

$$\frac{k_l}{K_{\text{eff}}} = \frac{1}{\ln(r_w/r_v)}\left\{\left[\frac{k_l}{k_w}\right]\left[\ln\frac{r_w}{r_w - 2r_c - 2r_{ws}} + \ln\frac{r_v + 2(n-1)r_c(1+r_{ws}/r_c)}{r_v}\right] + \ln\frac{r_w - 2r_c(1+r_{ws}/r_c)}{r_v + 2(n-1)r_c(1+r_{ws}/r_c)}\right\} \tag{15}$$

where

$$\frac{k_w}{k_l} = 1\Big/\left[\frac{r_c}{r_{ws}}+1\right]\left[2\frac{k_l}{k_s} + \left(\frac{r_c}{r_{ws}} - 1\right)\right] + 2\Big/\left[\frac{r_c}{r_{ws}}+1\right]\left[\frac{k_l}{k_s}\left(\frac{r_{ws}}{r_c}+1\right)\right] + 1\Big/\left[\frac{r_{ws}}{r_c}+1\right]^2 \tag{16}$$

This effective thermal conductivity model is developed in Ref. 14.

Evaporator Section

The fluid flow in the evaporator is modeled as vapor flowing out of a porous wall (wick surface) into a vapor cavity with make-up liquid being supplied through the wick. The wick length is divided into two regions, one with liquid flowing, and one filled with static vapor (see Fig. 6). For a given active length, a simple pressure balance[14] shows that the same meniscus radius must exist at both axial and radial interfaces. Hence the active length (L_e) will vary with the meniscus radius if the pore size in the axial direction is greater than the pore size in the radial direction (r_c). This reasoning suggests that, for a given wick, a function exists where

$$L_e/l_e = \text{function}[r_m/r_c] \tag{17}$$

Consideration of the data taken in this study (see Fig. 7) suggests the relation

$$L_e/l_e = 0.656[r_m/r_c - 1]^{0.107} \tag{18}$$

for

$$r_c\langle\text{radial}\rangle < r_c\langle\text{axial}\rangle \tag{19}$$

and

$$L_e/l_e = 1.0 \tag{20}$$

for

$$r_c\langle\text{radial}\rangle \geqq r_c\langle\text{axial}\rangle \tag{21}$$

The constants in Eq. (18) apply only to the wick tested in this investigation. Although other capillary structures may use the same wick configuration (i.e., cylindrical wrappings of layers of mesh screen), variations are possible in wrapping tightness and therefore in liquid gaps between the screen layers. The active length L_e, used in Eq. (18), was evaluated from measured heat-transfer rate and vapor and outer shell wall temperatures. The ratio (r_m/r_c) was evaluated from Eq. (6) in conjunction with Eq. (10).

The existence of curvature on the evaporator liquid-vapor interface suggests a radial retreat of the interface into the wick, similar to the partial saturation reported by Roberts[9] and Chun.[3]

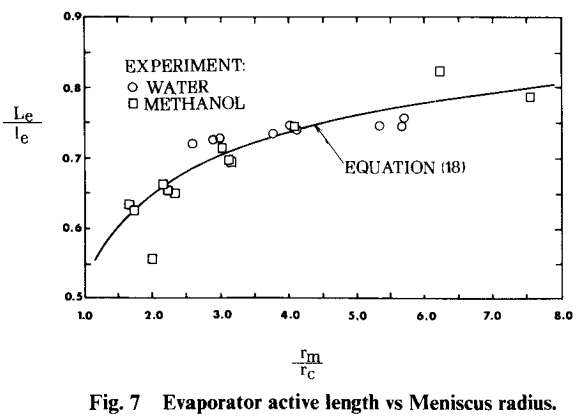

Fig. 7 Evaporator active length vs Meniscus radius.

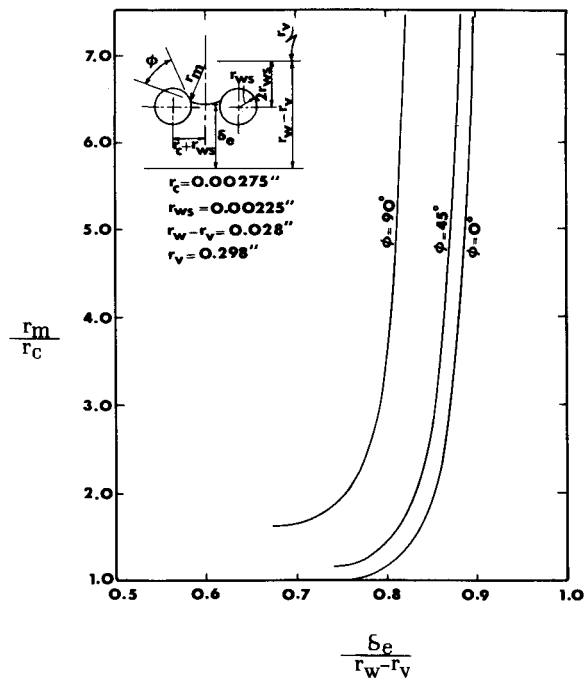

Fig. 8 Meniscus radius vs effective wick thickness in evaporator.

This radial retreat is characterized by the effective wick thickness δ_e (see Fig. 8). The interface position required by Eq. (7) is given by

$$r_{ve} = r_w - \delta_e \tag{22}$$

where δ_e depends on the operating meniscus radius, the detailed wick geometry (including the radius of the screen wire r_{ws}), and the fluid contact angle. Typical values of δ_e based on the geometry used in the heat pipe tested are indicated in Fig. 8.

The heat flow path for the evaporator is modeled as simple radial conduction through the active length of the wick and the combination of axial and radial conduction in the heat pipe shell. Thus in Eq. (7), $\dot{Q}_e$ is taken to be independent and $\bar{T}_{ew}$ is taken to be dependent and

$$\dot{Q}_e = \text{external power supplied} \tag{23}$$

System of Equations and Dimensionless Groups

Equations (6, 10, 14–17, and 23) form a system of six equations with six dependent variables. Written in dimensionless form, these equations are

$$\frac{r_m}{r_c} = 2\left[\frac{\rho_l \sigma h_{vl}}{\mu_l}\right]\left[\frac{\pi r_c^2}{\dot{Q}_e}\right]\left[\frac{(r_w/r_v)^2-1}{(r_c/r_v)^2}\right] \Big/ Kr_c l_c\left[\frac{1}{2}\left(\frac{L_e}{l_e}\right)\frac{l_e}{l_c} + \frac{l_a}{l_c} + \frac{1}{2}\frac{L_c}{l_c}\right] \tag{24}$$

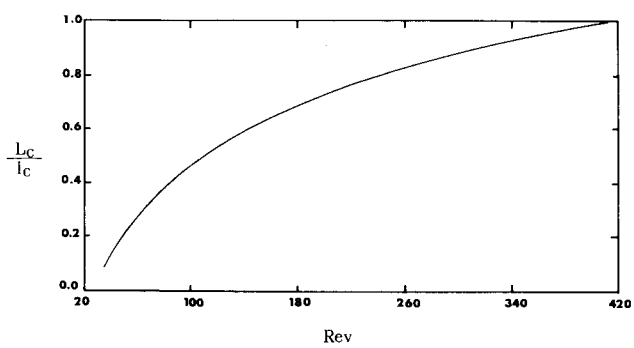

Fig. 9 Predicted condenser active length vs axial vapor Reynolds number.

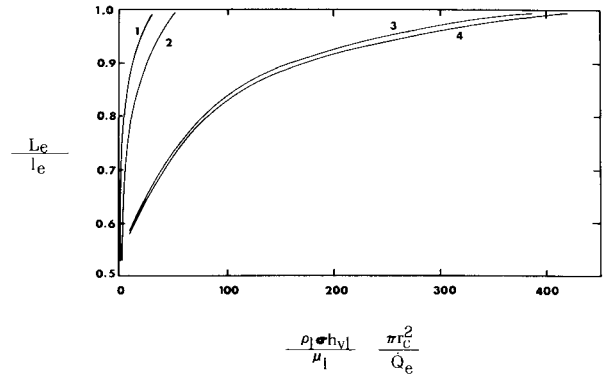

Fig. 10 Predicted evaporator active length vs heat pipe number.

$$\frac{T_o}{T_c} = 1 + \left[\frac{\dot{Q}_e}{2\pi r_w l_c U_c T_c}\right]\frac{l_c}{L_c}\left\{1 + \left[\frac{U_c l_c}{K_s}\right]\left[\frac{r_w}{r_v}\right]\left[\frac{r_v}{l_c}\right]\left[\frac{K_s}{K_l}\right]\left[\frac{K_l}{K_{\text{eff}}}\right]\ln\left(\frac{r_w}{r_v}\right)\right\} \tag{25}$$

$$L_c/l_c = f_1[(2/\pi)(\dot{Q}_e/h_{vl} r_v \mu_v)] \tag{26}$$

$$L_e/l_e = f_2[r_m/r_c] \tag{27}$$

$$\delta_e/(r_w - r_v) = f_3[r_m/r_c, r_w/r_v, r_{ws}/r_c, r_c/r_v, \phi] \tag{28}$$

and

$$K_e/K_{\text{eff}} = f_4[r_w/r_v, r_{ws}/r_c, r_c/r_v, K_s/K_l, n] \tag{29}$$

where f_1 is given by Eq. (10), f_2 by Eq. (18), f_3 by plot of Fig. 8, and f_4 by Eq. (15) with substitution of Eq. (16).

For the 24 variables in these equations, there correspond 20 dimensionless groups. Independent groups include the parameters of fixed geometry, fluid properties, and the external factors of condenser sink temperature, condenser unit conductance, and heat-transfer rate at the evaporator. Dependent groups are in the six terms on the left-hand side of Eqs. (24–29).

Results

With 14 independent groups, many plots of dependent vs independent groups are possible. Some of the more important relationships as computed from Eqs. (24–29) are shown in Figs. 9–14. Figure 9 indicates the variation of condenser active length with vapor Reynolds number. This length increases with increasing Reynolds number. For high Reynolds number, the length ratio becomes unity.

Figure 10 shows the variation of evaporator length with heat pipe number. This length is shown to increase with increased pipe number and to decrease slightly with increased vapor Reynolds number. Increases in design length and radius groups and the wick friction number cause a decrease in the active

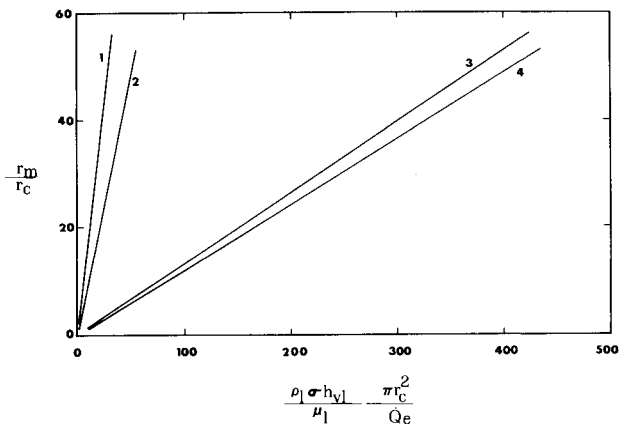

Fig. 11 Predicted evaporator Meniscus radius vs heat pipe number.

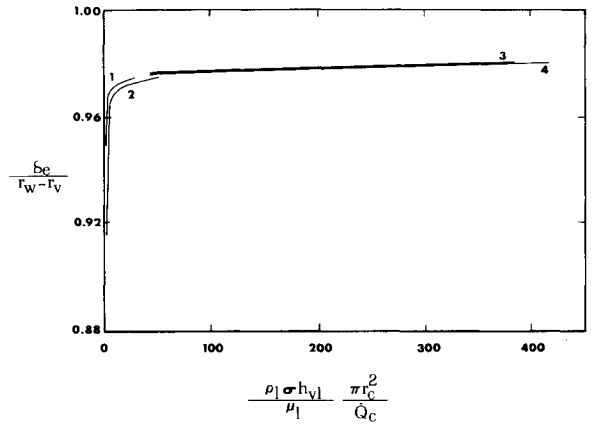

Fig. 12 Predicted evaporator effective wick thickness vs heat pipe number.

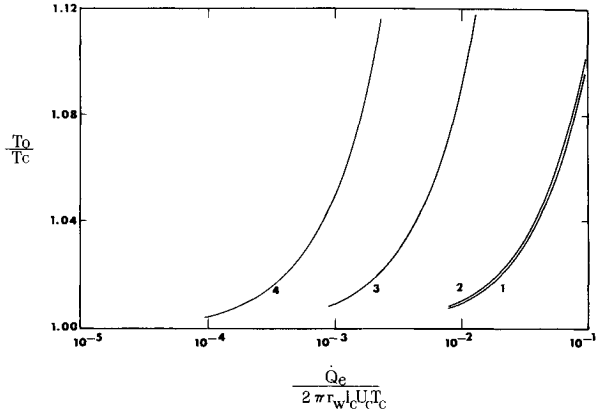

Fig. 14 Predicted heat pipe operating temperature vs condenser heat sink number.

Table 3 Dimensionless groups for Figs. 10, 11, and 12

Group	Definition	Curve 1	2	3	4
π_1	l_a/l_c	0.5	0.5	3.0	3.0
π_2	l_e/l_c	0.5	0.5	3.0	3.0
π_3	r_w/r_v	1.1	1.1	2.0	2.0
π_5	r_c/r_v	0.005	0.005	0.010	0.010
π_6	r_{ws}/r_c	0.5	0.5	1.0	1.0
π_7	$Kr_c l_c$	1×10^4	1×10^4	1×10^5	1×10^5
π_9	ϕ_o	0	0	$\pi/2$	$\pi/2$
π_{12}	$(2/\pi)(\dot{Q}_e/r_v \mu_v h_{vl})$	50	400	50	400

length ratio. Values of the other nondimensional groups used in the computations are listed in Table 3. These apply to Figs. 10–12.

Figure 11 indicates variation of evaporator meniscus radius with heat pipe number. The radius is shown to increase with increased pipe number and to decrease with increased vapor Reynolds number. Increases in design length and wick radius ratios and in the wick friction number cause a significant decrease in the meniscus radius ratio.

Figure 12 shows variation of evaporator wick thickness ratio with heat pipe number. This thickness increases sharply for low pipe numbers and increases slowly for large pipe numbers. An increase in vapor Reynolds number produces a slight decrease in thickness ratio. An increase in contact wetting angle produces a slight decrease in thickness ratio. Increases in length and wick radius ratios in addition to the wick friction number indicate an increase in the thickness ratio.

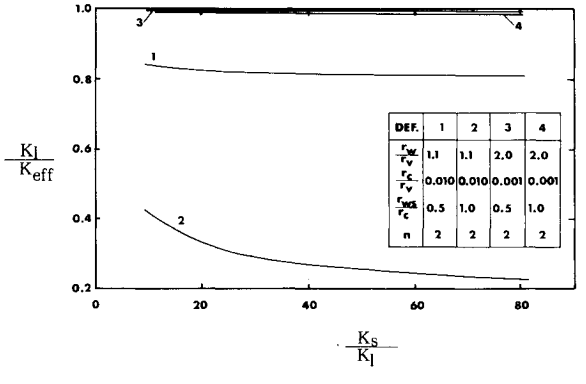

Fig. 13 Predicted wick effective conductivity vs wick solid-liquid conductivity ratio.

Figure 13 illustrates the dependency of the ratio of liquid conductivity to wick effective conductivity on the ratio of solid conductivity to liquid conductivity. The liquid to effective ratio decreases slowly with increasing solid/liquid ratio. The liquid/effective conductivity ratio decreases with increases in wick solid/pore radius ratios. The liquid/effective conductivity ratio increases with combined increase in wick radius ratio and decrease in wick-pore/vapor space radius ratios.

Figure 14 shows the variation of heat pipe operating temperature with condenser environment number. The vapor temperature ratio increases with increased condenser environment number, decreases with increased heat sink number and decreases with increased wick radius number. Values of the other

Table 4 Dimensionless groups for Fig. 14

Group	Definition	Curve 1	2	3	4
π_3	r_w/r_v	1.01	1.01	1.10	1.10
π_4	r_v/l_c	0.01	0.01	0.10	0.10
π_5	r_c/r_v	0.001	0.001	0.01	0.01
π_6	r_{ws}/r_c	0.5	0.5	1.0	1.0
π_8	n	2	2	2	2
π_{10}	K_s/K_l	10	10	80	80
π_{12}	$(2/\pi)(\dot{Q}_e/r_v \mu_v h_{vl})$	400	400	50	50
π_{14}	$U_c l_c/K_s$	5	50	5	50

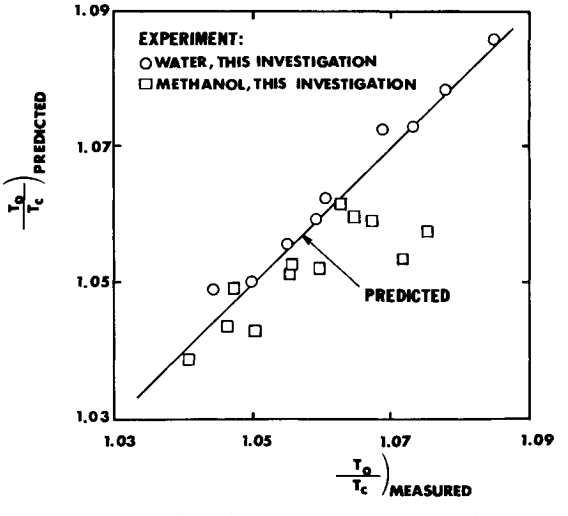

Fig. 15 Comparison of predicted and measured heat pipe operating temperature.

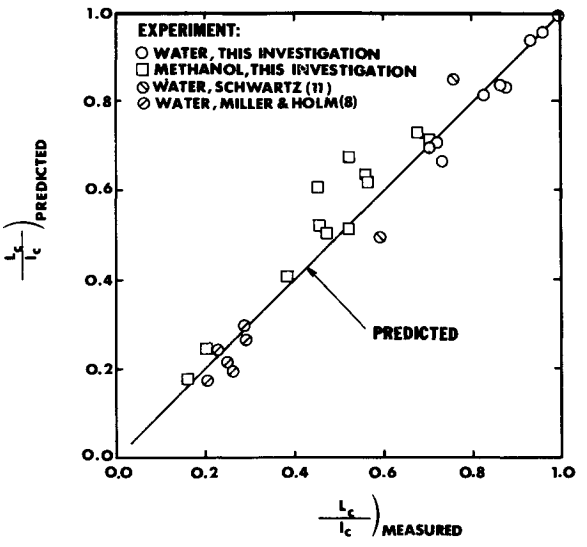

Fig. 16 Comparison of predicted and measured condenser active length.

nondimensional groups used in computations of values for the various curves shown on Fig. 14 are listed in Table 4.

Comparisons between predicted and measured parameters are shown in Figs. 15–17. Predicted values were obtained from solutions of Eqs. (24–29) and measured values are evaluated from measured parameters (e.g., wall and vapor temperatures and heat-transfer rates). These comparisons agree to within 15%. Figure 15 indicates agreement between measured and predicted values of the ratio of heat pipe operating temperature to condenser temperature. Figure 16 shows agreement for the ratio of condenser active length to design length. Included are data reduced from the experimental measurements of Miller[8] and Schwartz.[11] These works used horizontal water heat pipes with wicks similar to that tested in this study. Figure 17 depicts the agreement for the ratio of evaporator active length to design length. Data of other investigators are not indicated due to incomplete data reporting and employment of wick wrapping geometry different from that tested in this investigation. Sufficient data was reported by Fox[5] to indicate that his evaporator length did vary (see also Ref. 14).

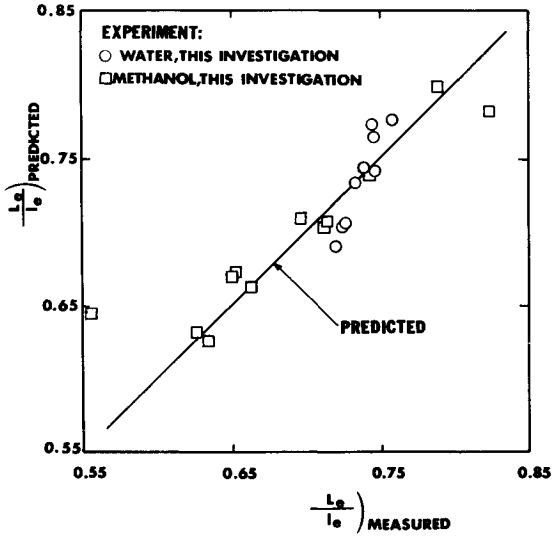

Fig. 17 Comparison of predicted and measured evaporator active length.

Conclusions

For the ranges of variables studied in this investigation, the significant conclusions are:

1) Although the axial pressure drop of the vapor is negligible, vapor dynamics are important. Variation of the axial vapor Reynolds number effects the active length of condensation. Corresponding to this length change is a variation in the over-all thermal resistance of the heat pipe.

2) Variation of the evaporator meniscus radius for different heat pipe operating points (below the capillary limited maximum heat rate) may reflect variations of the active length of evaporation. This dependency should exist only when nonisotropic wick geometrical configurations are employed, e.g., when pore radii within the wick are larger than the pore radius on the wick surface. Corresponding to the length change there exists a section in which the wick is void of liquid and energy transfer is by axial conduction in the heat pipe shell. Also corresponding to this length change is a variation in the over-all thermal resistance of the heat pipe.

3) The significance of the wick-solid radius r_{ws} is reflected in variation of the effective thickness of the wick δ_e and variation of the wick effective thermal conductivity. These variations also cause changes in the over-all thermal resistance of the heat pipe.

4) The design of a heat pipe should include consideration of active condenser length and active evaporator length.

References

[1] Bankston, C. A. and Smith, H. J., "Incompressible Laminar Vapor Flow in Cylindrical Heat Pipes," Paper 71-WA/HT-15 presented at the ASME Winter Annual Meeting, Washington, D.C., Nov. 1971.

[2] Chi, S. W. and Cygnarowicz, T. A., "Theoretical Analysis of Cryogenic Heat Pipes," Paper 70-HT/Sp-6, presented at the ASME Space Technology and Heat Transfer Conference, Los Angeles, Calif., June 1970.

[3] Chun, K. R., "Some Experiments on Screen Wick Dry-Out Limits," Paper 71-WA/HT-6, presented at the ASME Winter Annual Meeting, Washington, D.C., Nov. 1971.

[4] Cotter, T. P., "Theory of Heat Pipes," LA-3246-MS, March 1965, Los Alamos Scientific Lab., Los Alamos, Calif.

[5] Fox, R. D., Carothers, K. G., and Thompson, W. J., "Internal Temperature Distributions in an Operational Heat Pipe," *AIAA Journal*, Vol. 10, No. 7, July 1972, pp. 859–860.

[6] Kunz, H. R., Langston, L. S., Hilton, B. H., Wyde, S. S., and Nashick, G. H., "Vapor-Chamber Fin Studies, Transport Properties and Boiling Characteristics of Wicks," CR-812, June 1967, NASA.

[7] Kunz, H. R., Wyde, S. S., Nashick, G. H., and Barnes, J. F., "Vapor-Chamber Fin Studies, Operating Characteristics of Fin Models," CR-1139, Aug. 1968, NASA.

[8] Miller, P. L. and Holm, F. W., "Investigation of Constraints in Thermal Similitude," Vol. II, AFFDL-TR-69-91, Dec. 1969, Air Force Flight Dynamic Lab., Wright-Patterson Air Force Base, Ohio.

[9] Roberts, C. C. and Felderman, K. T., Jr., "Predicting Performance of Heat Pipes with Partially Saturated Wicks," Paper 72-WA/HT-38 presented at the ASME Winter Annual Meeting, New York, Nov. 1972.

[10] Scheidegger, A. E., *The Physics of Flow Through Porous Media*, Macmillan, New York, 1960, p. 112.

[11] Schwartz, J., "Performance Map of the Water Heat Pipe and the Phenomenon of Noncondensible Gas Generation," Paper 69-HT-15 presented at the ASME-AIChE Heat Transfer Conference, Minneapolis, Minn., Aug. 1969.

[12] Shinnick, W. A., "Heat Pipe Technology, A Bibliography with Abstracts," Cumulative Vols., March 1971 Sept. 1972, Technology Application Center, University of New Mexico, Albuquerque, N. Mex.

[13] Sun, K. H. and Tein, C. L., "Simple Conduction Model for Theoretical Steady-State Heat Pipe Performance," *AIAA Journal*, Vol. 10, No. 8, Aug. 1972, pp. 1051–1057.

[14] Williams, C. L., "Correlation of Heat Pipe Parameters," Ph.D. thesis, March 1973, Dept. of Mechanical Engineering, Georgia Institute of Technology, Atlanta, Ga.

[15] Winter, E. R. F. and Borsch, W. O., "The Heat Pipe," *Advances in Heat Transfer*, Vol. 7, 1971, p. 219.